lubricants

MDPI

Article

Modeling and Validation of the Sealing Performance of High-Pressure Vane Rotary Actuator

Yi Wu [1], Junjie Zhou [1,2,*], Wenjie Ma [3] and Wenbo Liao [1]

[1] National Key Laboratory of Vehicular Transmission, Beijing Institute of Technology, Beijing 100081, China
[2] Institute of Advanced Technology, Beijing Institute of Technology, Jinan 250101, China
[3] Inner Mongolia First Machinery Group Co., Ltd., Baotou 014030, China
* Correspondence: bit_zhou50082@163.com

Abstract: The EHRA (Electro-Hydraulic Rotary Actuator), using a vane rotary actuator, has the advantages of a high torque density and integration and is expected to become a joint actuator for robots. This research focuses on the sealing characteristics of various parts of a vane rotary actuator. The average Reynolds equation was used to analyze the leakage characteristics at the gap. A detailed theoretical analysis was conducted on the internal leakage mechanism of a vane rotary actuator using an X-ring as the dynamic seal for the rotor vane. According to the path of internal leakage, different sealing forms are considered as a series or parallel, and the Newton iteration method is used to obtain the total internal leakage characteristics of a vane rotary actuator. It was also considered that the deformation of the vane rotary actuator caused a thicker gap, leading to an increase in internal leakage. The calculation results are consistent with the experimental data. The analysis results indicate that when estimating the internal leakage of a vane rotary actuator, it is necessary to take the pressure of the high-pressure chamber and output shaft position as inputs. This research provides a reference for an analysis of the method of internal leakage for vane rotary actuators. It provides theoretical support for designing a vane rotary actuator with more minor internal leakage and a higher volumetric efficiency.

Keywords: vane rotary actuator; X-ring; average Reynolds equation; elastohydrodynamic lubrication; reciprocating seal

Citation: Wu, Y.; Zhou, J.; Ma, W.; Liao, W. Modeling and Validation of the Sealing Performance of High-Pressure Vane Rotary Actuator. *Lubricants* **2024**, *12*, 381. https://doi.org/10.3390/lubricants12110381

Received: 26 July 2024
Revised: 14 October 2024
Accepted: 29 October 2024
Published: 2 November 2024

1. Introduction

The emergence of the EHA (electro-hydraulic actuator) combined the advantages of hydraulic and electric transmission to achieve a distributed electro-hydraulic drive. The linear hydraulic cylinder requires additional space when driving the rotation of robot joints, and the moment arm of the linear actuator constantly changes when the robot joint angle changes. This results in significant differences in the load characteristics of the robot joints driven by the linear actuator at different angles, which is not conducive to the parameter matching design and the design of the control algorithms of the driving system. Taking the electro-hydraulic actuator with a vane rotary actuator as the driver of the robot joint not only avoids the additional space occupied by the actuator and improves the integration of the robot but it also makes it easier to design parameter matching and joint-compliant control algorithms, as its moment arm is not affected by changes in the output angle. It is expected to become a joint actuator for future mobile robot platforms.

The internal seal of the vane rotary actuator belongs to the reciprocating seal. Since the 1930s, many scholars have conducted experimental and theoretical research on reciprocating seals [1]. The elastohydrodynamic lubrication (EHL) theory is often used to analyze the sealing characteristics of elastic components [2]. When the EHL model is solved, the oil film thickness needs to be iterated repeatedly [3,4]. Based on the EHL theory, some scholars solved the initial numerical results of contact pressure distribution by a finite element

model [5–8]. An improved method for an EHL inverse solution proposed by G.K. Nikas solves the stability and convergence problems encountered in an EHL solution. The inverse solution adopts a mathematical derivation, and the film thickness distribution at the seal is directly calculated by the pressure distribution [9]. An EHL inverse solution is used to solve the sealing characteristics of vane rotary actuators [10,11]; it is also used to analyze the sealing characteristics of vane rotary actuators with a multi-layer material vane seal and obtain their sealing performance under different conditions of temperature, pressure, speed, and the pre-compression of elastic elements [12,13]. In addition to sealing with elastic elements, there are many installation gaps in the internal leakage path of a vane rotary actuator. The empirical formula of gap leakage can generally estimate the leakage of the gap. However, the gaps' forms are also different due to the differences in a vane rotary actuator's internal structure. In order to accurately analyze the sealing characteristics of the clearance part, the analytical model of the clearance part is constructed using the Reynolds equation. Several studies show that the sealing surface's roughness characteristics have a non-negligible impact on the sealing characteristics [14–18]. The average Reynolds equation theory proposed by Nadir Patir can consider the surface roughness characteristics of the two surfaces forming the gap [19,20]. The research on the sealing characteristics of a vane rotary actuator shows that the sealing gap changes with structural deformation [21], another factor that must be considered.

This paper focuses on the sealing characteristics of the vane rotary actuator, which adopts a combination seal, clearance seal, and X-ring star ring seal. In the calculation and analysis process, the average Reynolds equation is used to solve the clearance leakage, and the EHL inverse solution theory is used to solve the leakage at the X-ring seal in the middle of the rotor vane. Further, according to the internal leakage path, different sealing forms are regarded as a series or parallel, and the total internal leakage characteristics of the vane rotary actuator are obtained. The calculated results have a good match with the experimental data.

2. Structure of Vane Rotary Actuator

This paper focuses on a single vane rotary hydraulic actuator that can output a torque of about 270 N·m under a pressure of 15 MPa, with a total assembly mass of 3.3 kg and a high torque density. The main structure of the vane rotary actuator includes the front and rear end caps, cylinder body, output shaft, stator vane, and rotor vane. The rotor vane and stator vane divide the annular chamber formed between the cylinder body and output shaft into a high-pressure chamber and a low-pressure chamber, as shown in Figure 1. A sealing framework made of PEEK is installed in the middle of the rotor vane, and an X-ring installation groove is set in the sealing framework; the installation groove for the rollers and PTFE sealing block is set in the middle of the stator vane. The installation groove of a combined sealing structure composed of a PEEK sealing ring and O-ring is set at the contact position between the output shaft shoulder and the end caps of both sides; the end cap of the output shaft end is also equipped with a skeleton shaft seal to prevent leakage along the output shaft.

The stator vane is installed on the cylinder, and the top of the vane contacts with the output shaft. When the actuator is activated, the top of the stator vane will generate motion relative to the output shaft, which is the dynamic seal. The installation groove for the rollers and PEEK sealing blocks is set in the middle of the stator vane. The outer side of the sealing block is in contact with the roller, and the inner side is in contact with the output shaft. When high pressure is applied to one side of the vane rotary actuator, the roller rolls towards the other side, exerting a force on the sealing block. When the oil in the high-pressure chamber leaks into the low-pressure chamber through the stator vane, it first passes through the gap formed between the stator vane and the output shaft, through the contact position between the sealing block and the output shaft or the gap formed between the sealing block and the end caps of both sides; then it passes through

the gap formed between the stator vane and the output shaft; and finally it reaches the low-pressure chamber.

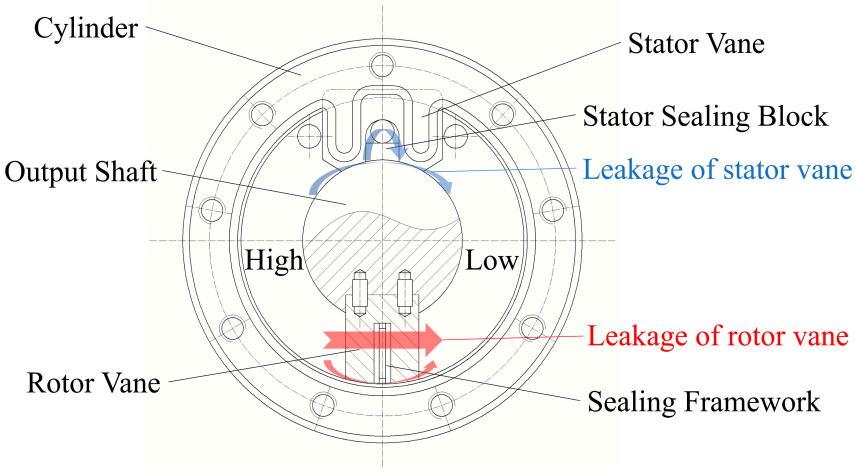

Figure 1. Main structure of vane rotary actuator.

The structure of a rotor vane is shown in Figure 2. A rotor vane is installed on an output shaft and follows the rotation of the output shaft. When the actuator is activated, the top of the rotor vane will generate motion relative to the cylinder, which is the dynamic seal. The advantage of the X-ring, compared to the O-ring, is that the star-shaped sealing ring forms a lubrication cavity between the sealing lips, which has minor friction resistance; the casting fin is in the concave part of the cross-section; and the noncircular sections can avoid rolling during reciprocating motion. The X-ring surrounds the sealing framework, and the rounded corners formed at the sharp corners cannot fully fit the sealing surface, resulting in corner gap leakage, as shown in Figure 3.

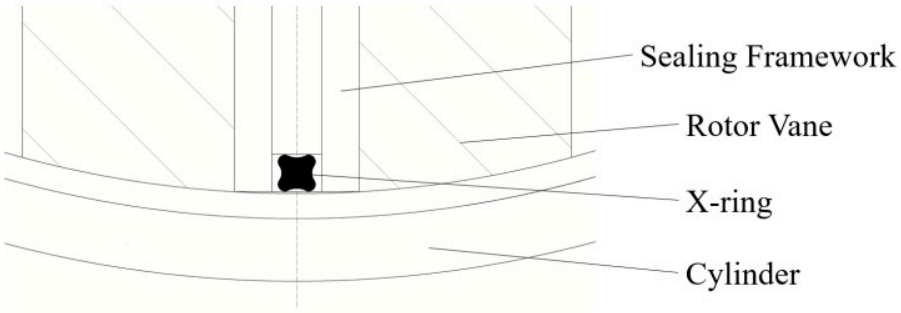

Figure 2. Sealing structure of rotor vane.

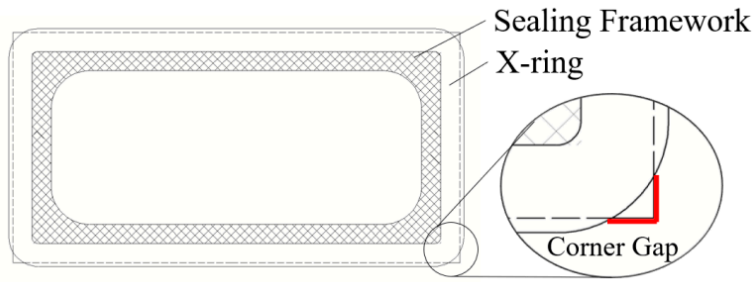

Figure 3. Corner gap of rotor seal.

When the oil in the high-pressure chamber leaks into the low-pressure chamber through the rotor vane, it first passes through the gap between the rotor vane and the cylinder or between the rotor vane and the end caps of both sides. Then, it passes through the X-ring or corner gap, through the gap formed between the rotor vane and the cylinder or between the rotor vane and the end caps of both sides, and finally it reaches the low-pressure chamber. In relation to the internal leakage of a vane rotary actuator, leakage of the rotor vane is the main problem.

3. Sealing Analysis Model

The average Reynolds equation is used to solve the gap leakage, and the X-ring seal in the middle of the vane is solved using the EHL inverse solution theory. Based on the path of the internal leakage, consider the different sealing forms as a series or parallel, and use Newton's iteration method to determine the pressure at the middle position. Finally, obtain the total internal leakage of the vane rotary actuator.

3.1. Gap: Average Reynolds Equation

In order to reduce the internal leakage of the vane rotary actuator, the clearance of the internal structure needs to be strictly controlled, usually between 5 and 50 μm. In a small gap, the relative velocity and surface roughness of the two surfaces in the gap can affect the flow state of the fluid. The Reynolds equations at different gap positions are constructed to solve the internal leakage in the gap. The steady-state Reynolds equation is shown in Equation (1):

$$\frac{\partial}{\partial x}\left(\frac{\partial p}{\partial x}\frac{h^3}{12\mu}\right) = \frac{u}{2}\frac{\partial h}{\partial x} \tag{1}$$

According to Newton's law of internal friction, the viscous friction force acting on the gap surface can be expressed as Equation (2):

$$\tau = \left(-\mu\frac{\partial v}{\partial z}\right)_{h=h_b} \tag{2}$$

$$F = \iint \tau \mathrm{d}A \tag{3}$$

The leakage flow rate per unit width can be expressed as Equation (4):

$$Q = \iint v\mathrm{d}z\mathrm{d}x \tag{4}$$

The average Reynolds equation considers the influence of the surface characteristics, and the pressure flow factor φ_x and shear flow factor φ_s are introduced.

$$\frac{\partial}{\partial x}\left(\varphi_x\frac{\partial p}{\partial x}\frac{h^3}{12\mu}\right) = \frac{u}{2}\frac{\partial h}{\partial x} + \frac{u}{2}\sigma\frac{\partial \varphi_s}{\partial x} \tag{5}$$

Ignore the transient terms; φ_x is the factor of pressure flow, which represents the influence of surface roughness on liquid flow in the gaps; and φ_s is the factor of shear flow, indicating that the surface roughness wave valley drives the flow of liquids. Two factors are calculated using Equations (6) and (7):

$$\varphi_x = 1 - 0.9e^{-0.56H} \tag{6}$$

$$\varphi_s = V_{r1}\varnothing_s\left(\frac{h}{\sigma}, \gamma_1\right) - V_{r2}\varnothing_s\left(\frac{h}{\sigma}, \gamma_2\right) \tag{7}$$

where $H = h/\sigma$ is the ratio between oil film thickness and the standard deviation of surface roughness. As H increases, φ_x approaches one. In this paper, $H > 1$; $\sigma = \sqrt{\sigma_1^2 + \sigma_2^2}$ is the root mean square value of the standard deviation of the distribution of the two surfaces'

roughness where $V_{ri} = \left(\frac{\sigma_i}{\sigma}\right)^2$; γ represents the directional characteristics of the surface roughness distribution; and $\gamma = 1$ denotes an isotropic surface. In this paper, the roughness of the two surfaces is taken as Ra3.2, and they are all isotropic surfaces. $\varnothing_s$ is a parameter related to H. As H increases, $\varnothing_s$ approaches 0, $\varnothing_s$ is calculated using Equation (8).

$$\begin{cases} \varnothing_s = 1.899H^{0.98}e^{-0.92H+0.05H^2} & H \le 5 \\ \varnothing_s = 1.126e^{-0.25H} & H > 5 \end{cases} \tag{8}$$

The calculation formula for the flow rate is as follows:

$$\overline{Q}_x = -\varphi_x \frac{h^3}{12\mu}\frac{\partial \overline{p}}{\partial x} + \frac{u}{2}\overline{h}_T + \frac{u}{2}\sigma\varphi_s \tag{9}$$

In the average Reynolds equation, the average shear stress can be represented by Equation (10).

$$\overline{\tau} = \mu\frac{u}{h}(\varphi_f \pm \varphi_{fs}) \pm \varphi_{fp}\frac{h}{2}\frac{\partial \overline{p}}{\partial x} \tag{10}$$

The φ_f term arises from averaging the sliding velocity component of the shear stress; φ_{fs} is another correction term that arises from the combined effect of the roughness and sliding, similar to the φ_s term in mean flow; φ_{fp} is a correction factor for the mean pressure flow component of the shear stress, as H increases, φ_{fp} approaches one. These three factors are determined by H, V_{r1}, γ_1, V_{r2}, and γ_2.

$$\begin{cases} \varphi_f = \frac{35}{32}z\left\{(1-z^2)^3 ln\frac{z+1}{\frac{1}{300}} + \frac{1}{60}[-55 + z(132 + z(345 \right. \\ \quad \left. +z(-160 + z(-405 + z(60 + 147z)))))]\right\},\ H \le 3 \\ \varphi_f = \frac{35}{32}z\left\{(1-z^2)^3 ln\frac{z+1}{z-1} + \frac{z}{15}\left[66 + z^2\left(30z^2 - 80\right)\right]\right\},\ H > 3 \end{cases} \tag{11}$$

where $z = H/3$.

$$\varphi_{fs} = V_{r1}\varnothing_{fs}\left(\frac{h}{\sigma}, \gamma_1\right) - V_{r2}\varnothing_{fs}\left(\frac{h}{\sigma}, \gamma_2\right) \tag{12}$$

where $\varnothing_{fs} = 11.1H^{2.31}e^{-2.38H+0.11H^2}$.

$$\varphi_{fp} = 1 - 1.4e^{-0.66H} \tag{13}$$

After determining the factors in the average Reynolds equation and the thickness of the film in the gap is known, the over-relaxation iteration method is used to solve it. Finally, the thickness direction's pressure and velocity distribution are obtained. Furthermore, the gap's leakage and viscous friction force are calculated using Equations (9) and (10).

Three different gap thicknesses were set, with surface parameters set to an isotropic and surface roughness of Ra3.2. The leakage and horizontal viscous friction obtained by solving the Reynolds equation and average Reynolds equation were compared. The results are shown in Figure 4. The calculation results show that the smaller the film thickness, the more difference between the results calculated by the average Reynolds equation and the Reynolds equation, and the more influence by the surface roughness on the sealing characteristics. It can be seen that the results calculated by the average Reynolds equation vary more significantly with the relative velocity of the surface; that is, the sealing characteristics are more affected by the relative velocity of the surface when considering the surface roughness.

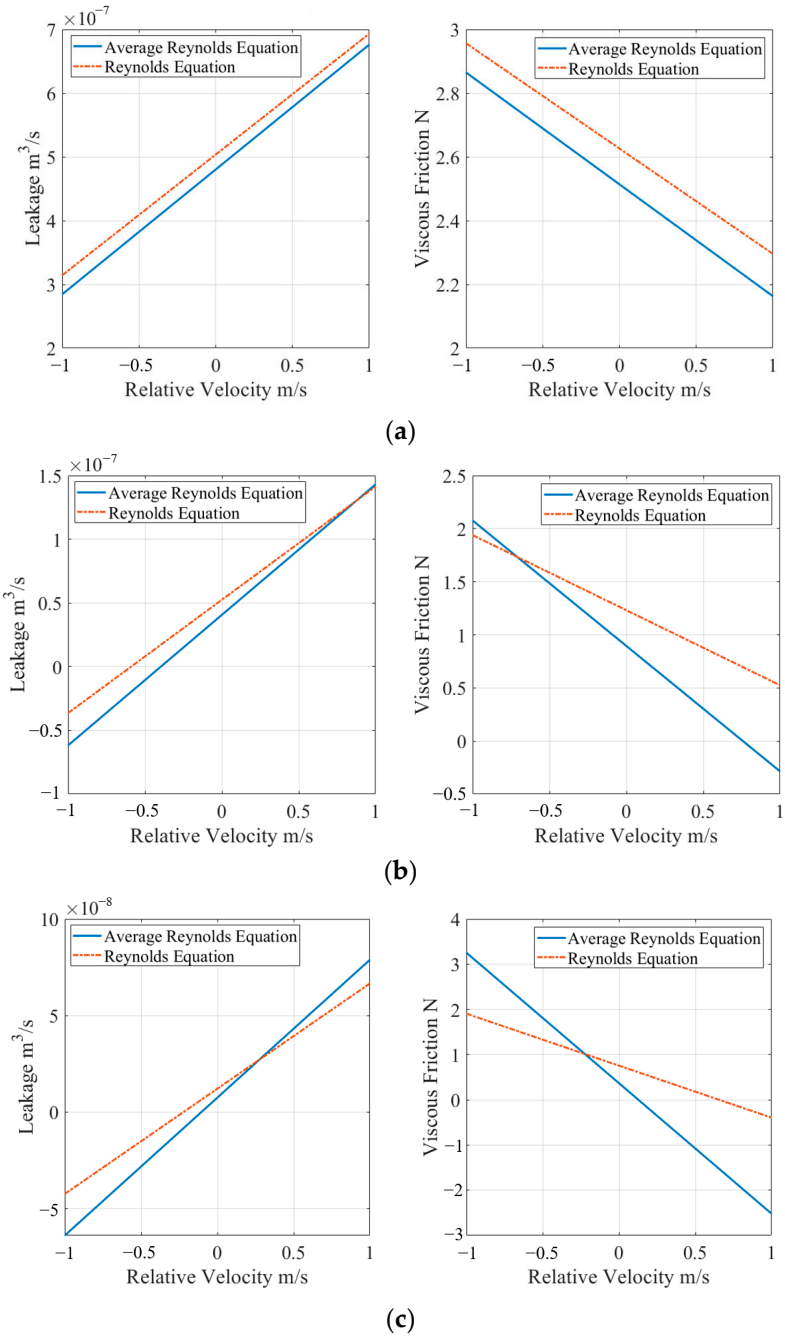

Figure 4. Comparison of calculation results between average Reynolds equation and Reynolds equation. (**a**) Comparison of 20 μm film thickness. (**b**) Comparison of 10 μm film thickness. (**c**) Comparison of 5 μm film thickness.

3.2. X-Ring: EHL Model

The sealing characteristics of the elastic element of the X-ring in the rotor vane in contact with the cylinder are calculated using the EHL inverse method, and the dry contact pressure is directly regarded as the EHL sealing pressure. The EHL needs to consider the oil's viscosity pressure relationship and density pressure relationship and is determined according to Equations (14) and (15):

$$\eta = \eta_0 e^{\alpha_B p} \tag{14}$$

$$\rho = \rho_0 [1 + C_a p / (1 + C_b p)] \tag{15}$$

According to Equation (16), the induced pressure q is obtained from the sealing pressure distribution.

$$\frac{\mathrm{d}q}{\mathrm{d}x} = \frac{1}{\eta\rho^2}\frac{\mathrm{d}p}{\mathrm{d}x} \tag{16}$$

Find the extreme point of induced pressure $x = x_\mathrm{m}$. At the extreme point, there is $\left.\frac{\mathrm{d}q}{\mathrm{d}x}\right|_{x=x_\mathrm{m}} = 0$; then, find the inflection point of induced pressure $x = x_\mathrm{a}$. At the inflection point, there is $\left.\frac{\mathrm{d}^2q}{\mathrm{d}x^2}\right|_{x=x_\mathrm{a}} = 0$, and the inflection point must be on the same side of the contact as the extremum point, on the ascending side of the pressure. After obtaining the extreme point and the inflection point, determine the film thickness h_m at the extreme point of induced pressure according to Equation (17). Calculate the film thickness of the X-ring sealing section by integrating it on both sides using Equation (18).

$$h_\mathrm{m} = \frac{2}{3}\rho_\alpha\sqrt{|2V\eta_\alpha/\mathrm{d}p(x_\mathrm{a})/\mathrm{d}x|} \tag{17}$$

$$\frac{\mathrm{d}h}{\mathrm{d}x} = \frac{\mathrm{d}^2q/\mathrm{d}x^2h^3}{6V - 3\mathrm{d}q/\mathrm{d}xh^2} \tag{18}$$

In the analysis of the X-ring sealing characteristics of the rotor vane, the finite element simulation method is used to obtain the contact pressure of the X-ring sealing. The X-ring of the elastic material adopts the Mooney–Rivlin hyperelastic model [22]. Firstly, the displacement load is applied to pre-compress the X-ring, and then the oil pressure is applied on the high-pressure side, finally obtaining the pressure distribution on the sealing surface, as shown in Figure 5.

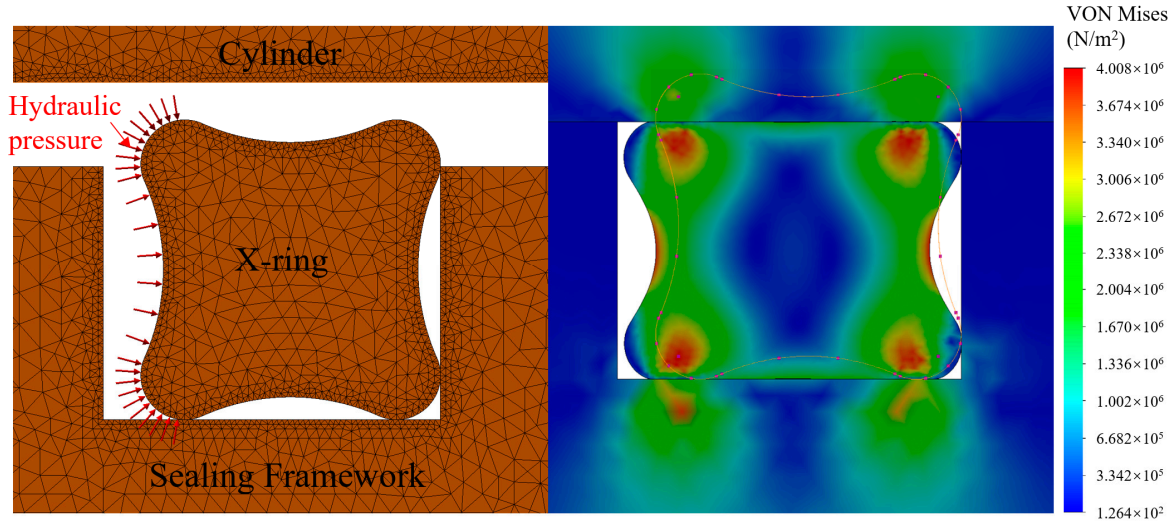

Figure 5. Finite element analysis of X-ring.

Figure 6 shows the surface contact pressure distribution under different sealing pressures. In addition, the influence of different pre-compression amounts on the contact pressure distribution should also be considered. A database of contact pressure distribution related to pre-compression and the sealing pressure was established through a series of simulation examples as input data for the inverse solution of the EHL sealing characteristics. Figure 7 shows the film thickness distribution and the contact pressure distribution at a sealing pressure of 8 MPa with a relative velocity of ±10 mm/s.

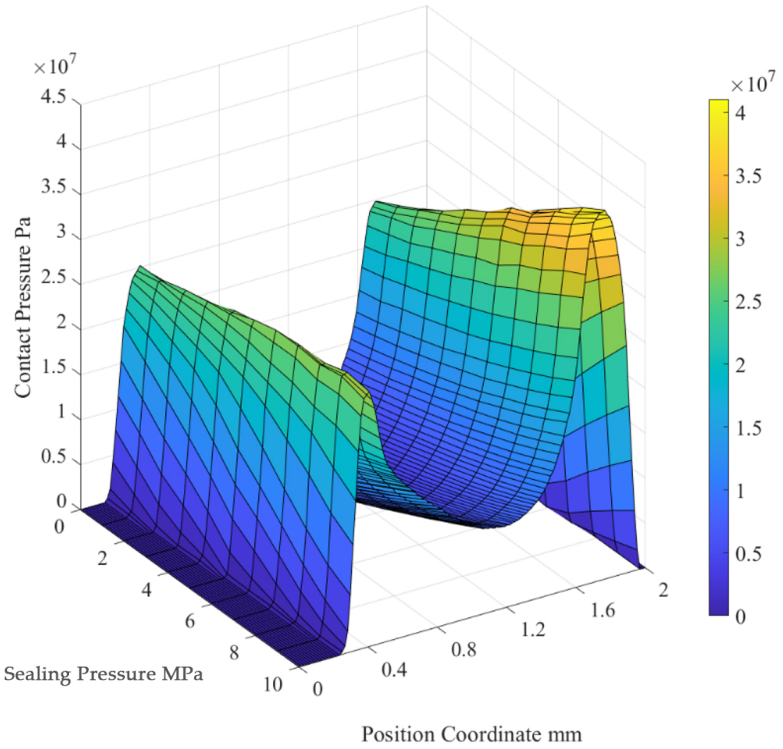

Figure 6. Contact pressure distribution of X-ring under different sealing pressures.

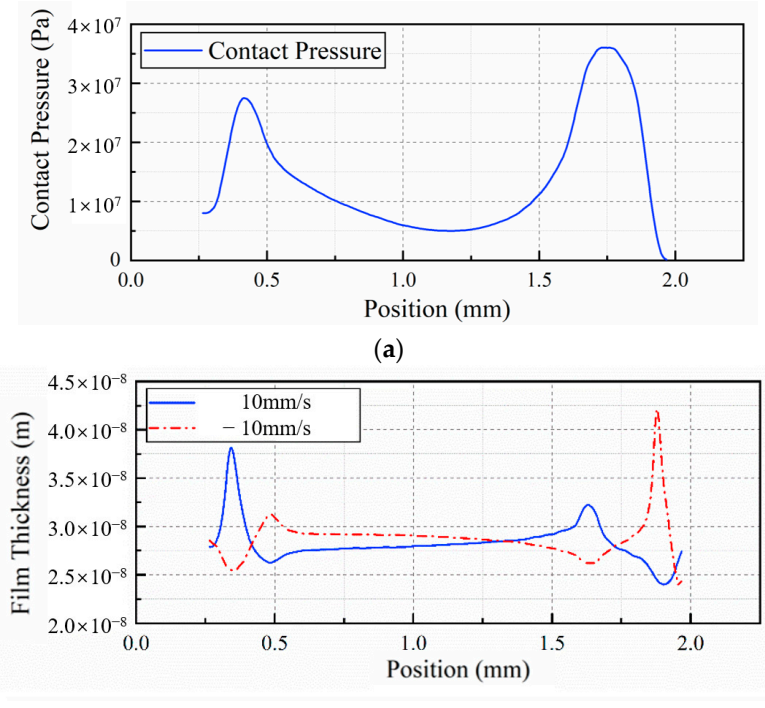

Figure 7. Pressure and film thickness distribution of X-ring seal. (**a**) Contact pressure of X-ring. (**b**) Film thickness of ±10 mm/s.

As the film thickness distribution is solved, the leakage and viscous friction can be calculated with Equations (3) and (4). The classic EHL theory considers the seal formed by the elastic materials with a circular cross-section. The pressure distribution in the inlet area gradually increases with the dynamic pressure, and after entering the contact area, the

pressure distribution is the same as that of dry contact. A necking phenomenon is formed in the outlet area, followed by a rapid decrease in pressure. There are two pressure peaks in the front and back of the X-ring, which can be seen as two circular cross sections with two inlet dynamic pressure zones and necking zones.

3.3. Multi-Stage Seal: Newton Iteration

As mentioned earlier in Figure 2, for the analysis of the sealing characteristics of the rotor vane, when the oil in the high-pressure chamber leaks into the low-pressure chamber, it needs to pass through a total of three seals. The first or third seal contains the gaps between the rotor vane and the cylinder and the gaps between the rotor vane and the end caps of both sides. The second seal contains the contact part between the X-ring and the cylinder, the contact part between the X-ring and the end caps of both sides, and the gap formed by the X-ring at a right-angle corner, as shown in Figure 3.

The leakage of the X-ring section will be calculated by solving the film thickness with the EHL inverse method. For the rest, the increased gap size is determined by pressure, and the size of the gap is the thickness of the film when the average Reynolds equation is solved, as shown in Figure 8.

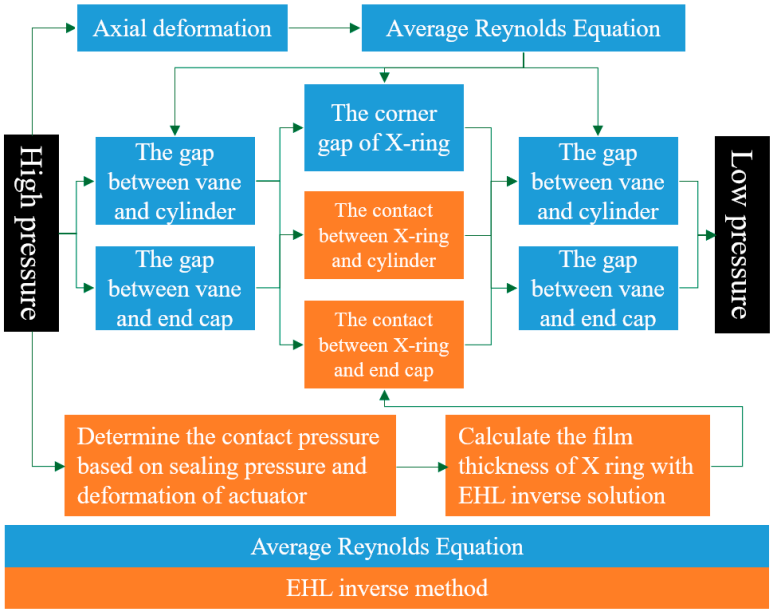

Figure 8. Flow chart diagram of the leakage calculation.

Take the seal between the top of the rotor vane and the cylinder as an example. The seal is divided into three sections with four pressure nodes. The first pressure node is the pressure of the high-pressure side, and the fourth pressure node is the pressure of the low-pressure side. With the flow conservation equation, the Newton iteration method is used to calculate the pressure values of the middle two nodes iteratively.

Assuming the pressures of the four nodes are P_1, P_2, P_3, P_4. The leakage of the first section is represented by $Q_1(P_1,\ P_2)$, and the leakage of the second section is $Q_2(P_2,\ P_3)$. Since the second seal is composed of two parts in parallel, it is considered that $Q_2(P_2,\ P_3) = Q_{21}(P_2,\ P_3) + Q_{22}(P_2,\ P_3)$. The leakage of the third section is $Q_3(P_3,\ P_4)$. Q_1 and Q_3 are obtained by solving the average Reynolds equation, Q_{21} by the Reynolds equation, and Q_{22} by the EHL inverse solution.

The system of flow conservation equation is as follows:

$$\begin{cases} F_1 = (Q_{21} + Q_{22}) - Q_1 \\ F_2 = Q_3 - (Q_{21} + Q_{22}) \end{cases} \tag{19}$$

The iterative formula of Newton's iteration method is as follows:

$$\begin{bmatrix} P_2 \\ P_3 \end{bmatrix}_{k+1} = \begin{bmatrix} P_2 \\ P_3 \end{bmatrix}_{k} - \begin{bmatrix} \frac{\partial F_1}{\partial P_2} & \frac{\partial F_1}{\partial P_3} \\ \frac{\partial F_2}{\partial P_2} & \frac{\partial F_2}{\partial P_3} \end{bmatrix}^{-1} \begin{bmatrix} F_1 \\ F_2 \end{bmatrix} \tag{20}$$

The calculation method for the elements in the Jacobian matrix in the equation is as follows:

$$\frac{\partial F_i}{\partial P_j} = \frac{F_i(P_j + \Delta P) - F_i(P_j)}{\Delta P} \tag{21}$$

After the iteration, the pressure distribution of this sealing section from the high-pressure node to the low-pressure node was obtained, as shown in Figure 8.

Comparing Figure 9b,c, a narrower sharp gap causes a more significant pressure drop and minor leakage during sealing. The leakage of the X-ring contact part is much more minor than the leakage of the corner gap, so the sealing effect of the second section seal of the rotor vane mainly depends on the width of the corner gap. Similar conclusions can be extended to the seal between the rotor vane and the end caps of both sides.

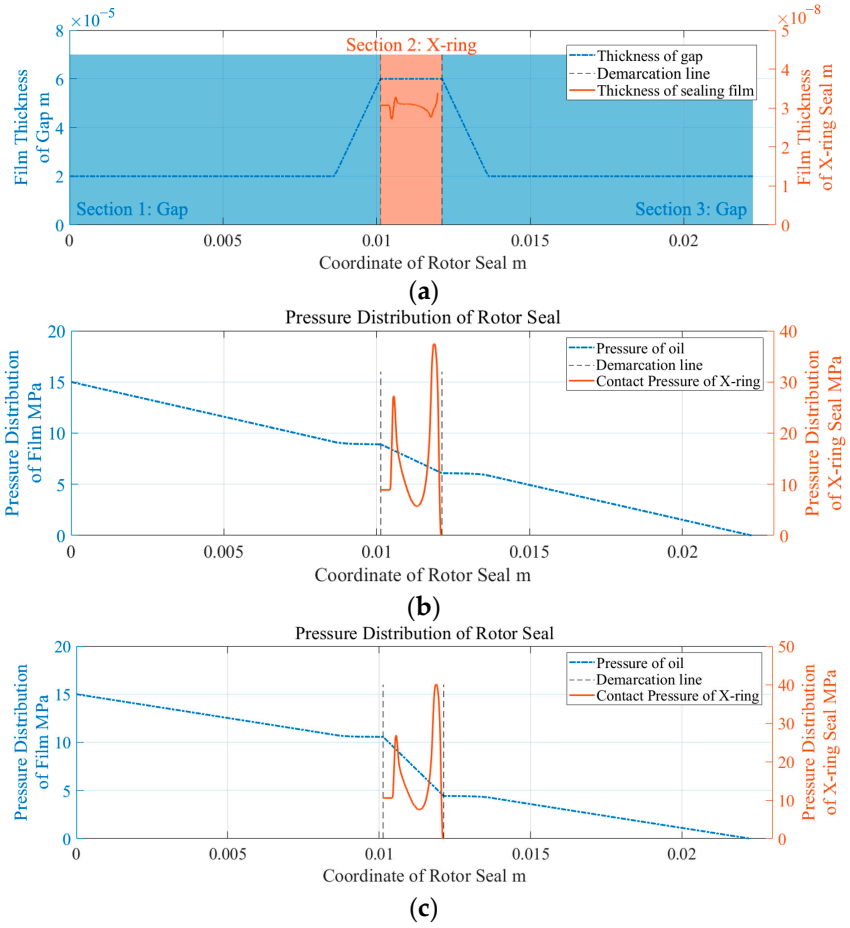

Figure 9. Film thickness and pressure distribution of rotor vane seal. (**a**) The film thickness distribution of the rotor vane seal. (**b**) The pressure distribution of the rotor vane with a corner gap width of 0.3 mm. (**c**) The pressure distribution of the rotor vane with a corner gap width of 0.1 mm.

In the sealing analysis of the stator vane, unlike with the rotor vane, the static seal is used between the stator vane and the end caps of both sides. A sealing ring is a reliable static seal, so the leakage between the stator vane and the end caps of both sides is not the main factor. The stator vane seal is divided into three seals, similar to those in the rotor vane. The first and third seal are the gap formed between the stator vane and the output

shaft; the second seal contains the surface between the sealing block and the output shaft and the gap between the sealing block and the end caps of both sides. All of them are solved using the average Reynolds equation.

The leakage at the shaft shoulder seal is much more minor than the direct internal leakage of the rotor and stator vanes, as verified in this experiment. Therefore, the leakage caused by the shaft shoulder seal is not considered in the total leakage.

In addition, to reduce the total assembly mass of the vane rotary actuator, the cylinder and end caps of both sides are made of an aluminum alloy material. That means that when the oil in the high-pressure chamber acts on the end caps and cylinder, it will cause an elastic deformation, as shown in Figure 9. Although this deformation is very small (often several tens of micrometers), it will lead to an increase in the sealing gap and have a significant impact on internal leakage. This is also the main nonlinear factor of internal leakage. Therefore, it is necessary to consider the increase in the gap caused by a deformation in the total leakage model.

Take the rotor vane as an example; the gap around the rotor vane before and after a deformation is treated as shown in Figure 10, i.e., the cylinder expands, and the center of the end cap protrudes outward. The magnitude of this elastic deformation is related to two factors: the pressure of the high-pressure chamber and the angle of the output shaft. The angle of the output shaft determines the volume of the high-pressure chamber inside the cylinder. The maximum limit condition for a deformation is when the pressure in the high-pressure chamber reaches a maximum of 15 MPa, and the high-pressure chamber occupies all the volume in the annular chamber except for the two blades. When calculating the actual sealing gap, multiply it by two factors: one is the pressure factor, and the other is the angle factor.

$$h_{\mathrm{T}} = h_{\mathrm{T}_0} + K_{\mathrm{p}} K_{\mathrm{a}} \left(h_{\mathrm{T}_{\max}} - h_{\mathrm{T}_0} \right) \tag{22}$$

where $K_{\mathrm{p}} = (p_{\mathrm{h}} / p_{\mathrm{h}_{\max}})^{\beta}$, and $K_{\mathrm{a}} = \theta / \theta_{\max}$. h_{T} is the size of the sealing gap in the current state. $h_{\mathrm{T}_{\max}}$ is the gap size of the extreme state, and h_{T_0} is the gap size of the initial no-load state. The exponential β reflects some of the nonlinear factors of a deformation caused by the pressure of the high-pressure chamber. For the configuration of the vane rotary actuator studied in this paper, $\beta = 3$.

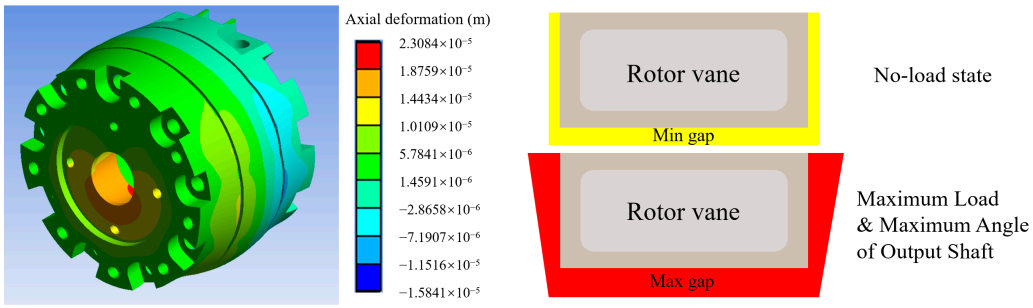

Figure 10. High-pressure deformation and increased sealing gap. (**a**) Finite Element Structure Analysis. (**b**) Increased gap around rotor vane.

4. Comparison of Experimental and Analysis Results

The composition of the experimental device is shown in Figures 11 and 12, and the main performance index of the device is shown in Table 1. The pressure of the system can be adjusted from 0 to 20 MPa, and the angle of the output shaft can be adjusted arbitrarily. The internal leakage is measured by the measuring cup method.

After taking into account the above factors, the state with the maximum output shaft angle is selected to obtain the internal leakage pressure curve of the vane rotary actuator, as shown in Figure 13. The experimental results of the total leakage are close to the theoretical analysis. Compared with the experimental results, the error of the theoretical analysis is

less than 5%. From the trend of the leakage curve in the figure, it can be seen that as the working pressure of the vane rotary actuator increases, the trend of leakage increasing is faster and faster. That is because the static pressure of the oil in the high-pressure chamber increases, leading to an increase in the thickness of the sealing gap, and exacerbating the increase in the internal leakage.

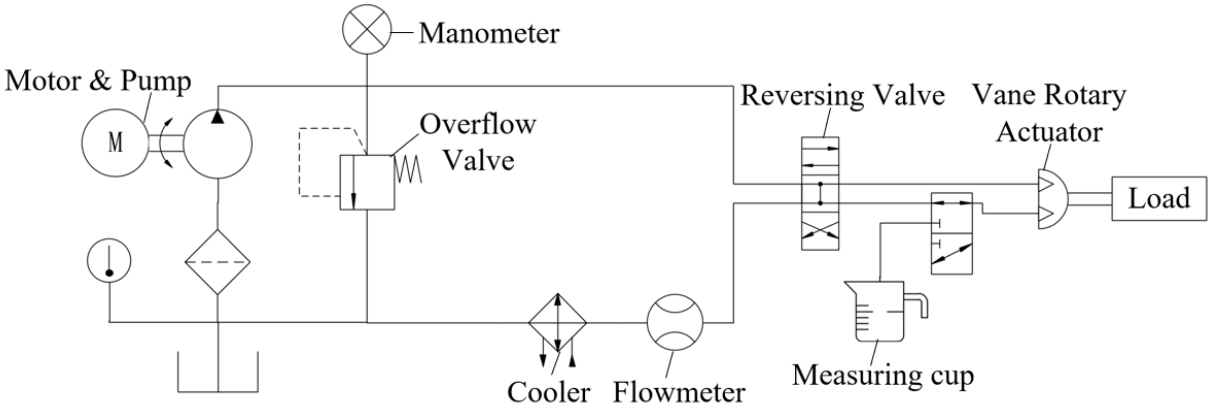

Figure 11. The composition of the experimental device.

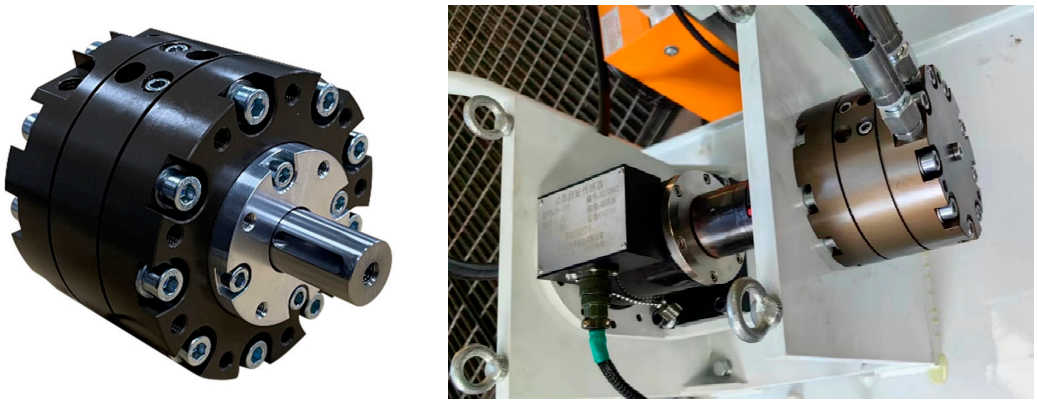

(**a**) (**b**)

Figure 12. Experimental device. (**a**) Vane rotary actuator. (**b**) Experimental bench.

Table 1. Performance index of vane rotary actuator.

Vane Rotary Actuator		Experimental Bench	
Working cavity volume	74 mL	Rated flow rate	6 L/min
Rated pressure	15 MPa	Working pressure	≥20 MPa
Rated torque	280 Nm	Power of motor pump	2 kW
Total mass	3.29 kg	Working medium	hydraulic oil 45
Torque density	85 Nm/kg		

In the internal leakage of the vane rotary actuator, the width of the dynamic sealing area of the rotor vane is the largest, and the internal leakage of the rotor vane is the main part of the internal leakage. The leakage at the sealing of the contact point between the rotor vane and the end caps is called end-face leakage. When the pressure is under 10 MPa, the leakage of the rotor vane accounts for about 50% of the total leakage; the end-face leakage does not exceed 0.03 L/min. However, when the pressure is high, due to the increase in the gap thickness, the end-face leakage increases rapidly, from 0.026 L/min with a pressure of 10 MPa to 0.34 L/min with a pressure of 15 MPa and becomes a significant part of the leakage of the rotor vane. As the pressure is 15 MPa, the total internal leakage is up to

0.9 L/min, and the leakage of the rotor vane is 0.61 L/min, which accounts for 68% of the internal leakage.

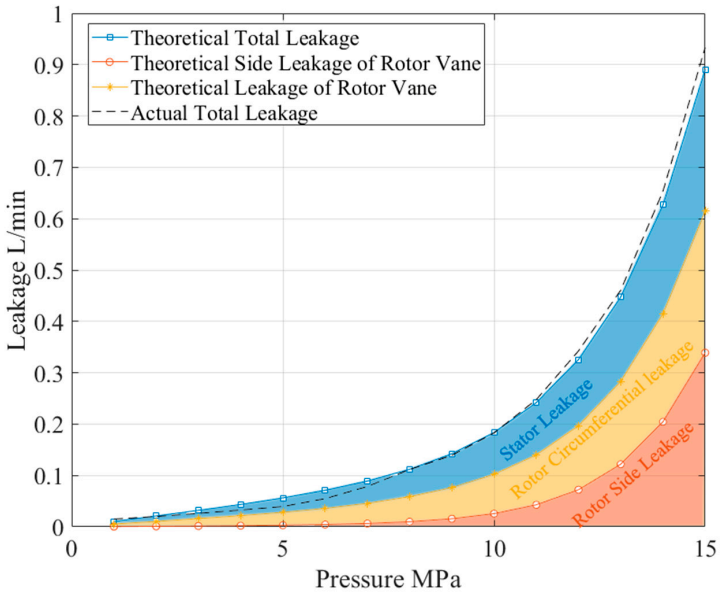

Figure 13. Internal leakage–pressure curve at maximum output shaft angle.

At a pressure of 15 MPa, change the angular position and angular velocity of the output shaft to obtain internal leakage data under different angular positions and velocities for the output shaft, as shown in Figure 14a. The impact of output shaft angular velocity on the internal leakage of the vane rotary actuator is very small. In contrast, the impact of the output shaft's angular position on the internal leakage of the vane rotary actuator is very significant. Therefore, when fitting or estimating the internal leakage of the vane rotary actuator, the pressure of the high-pressure chamber and output shaft position should be used as input conditions. The internal leakage at different pressures and output shaft positions is shown in Figure 14b.

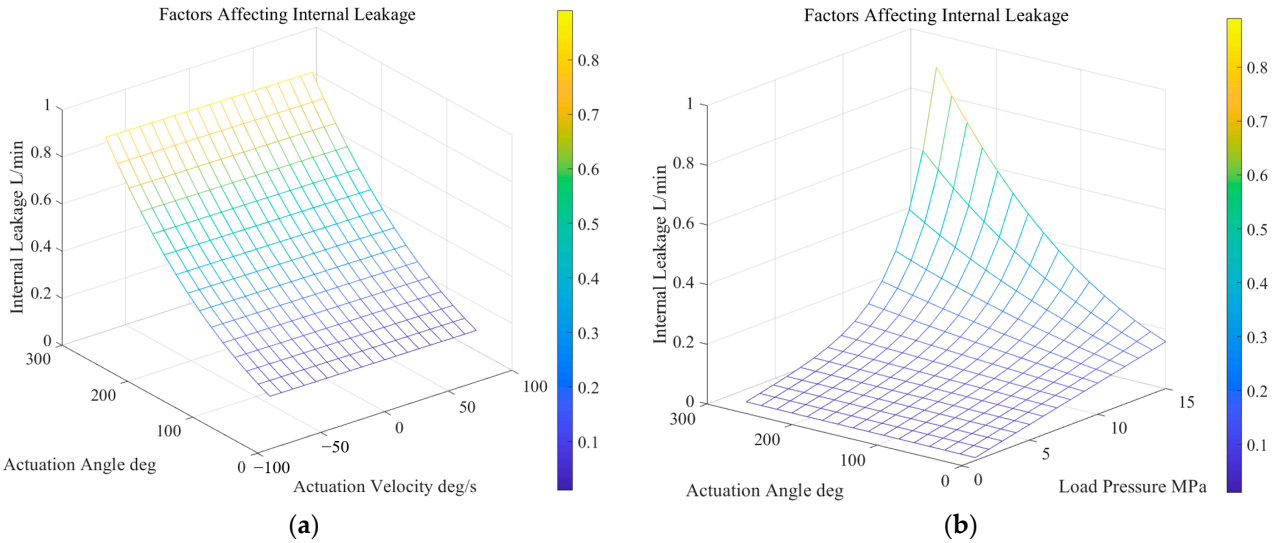

Figure 14. The impact of different factors on internal leakage. (**a**) The impact of shaft angle and angular velocity on internal leakage. (**b**) The impact of shaft angle and pressure on internal leakage.

5. Conclusions

This paper studies the sealing characteristics of a vane rotary actuator, and a model of the internal leakage is established. The main conclusions are as follows:

(1) The influence of surface roughness on the sealing characteristics is relatively significant for the gap of the dynamic seal of a vane rotary actuator (usually between 5 and 50 μm). The smaller the film thickness, the more significant the changes in pressure distribution with the changes in surface relative velocity. Therefore, the average Reynolds equation can provide a more accurate analysis of the small-thickness sealing gaps.

(2) Analyze the sealing characteristics of the X-ring seal through the EHL inverse solution and use the contact pressure distribution of the X-ring seal obtained by the finite element analysis method as the input condition of the EHL inverse solution to obtain the film thickness distribution of the X-ring contact part. The two pressure peaks of the X-ring can be seen as two circular cross-sections, with two inlet dynamic pressure zones and necking zones, respectively, and have minimal leakage, theoretically verifying the sealing performance of the X-ring.

(3) The oil in the high-pressure chamber of the vane rotary actuator will generate static pressure on the cylinder and end caps of both sides, causing an expansion and deformation of the cylinder and the end caps of both sides, increasing the sealing gap's thickness. The angle of the output shaft determines the high-pressure chamber volume, so a deformation of the end cap is also related to the angle position of the output shaft. The increase in the sealing gap thickness caused by a deformation is the main nonlinear factor for the internal leakage of a vane rotary actuator, and increasing the structural stiffness of vane rotary actuators must be considered.

(4) Segment different forms of seals, construct a flow conservation equation, and use the Newton iteration method to solve for the pressure value of the intermediate node to obtain the distribution of oil film pressure across the entire seal. Then, calculate the sum of the oil's internal leakage and viscous friction. The internal leakage pressure curve obtained is consistent with the experimental results. Compared to the output shaft angular velocity, the angular position of a vane rotary actuator plays an essential role in internal leakage that is more significant. When fitting or estimating the internal leakage of a vane rotary actuator, it is necessary to take the high-pressure chamber pressure and output shaft position as input conditions.

(5) The elastic element X-ring used in the sealing of a rotor vane often has a good sealing effect on the part it is in contact with, and the weak link in the sealing of a rotor vane lies in the non-contact part formed by the X-ring at the corner. The parts where the rotor vane comes into contact with the cylinder and the end caps on both sides are all dynamic seals. Thus, the leakage of a vane rotary actuator mainly comes from the rotor vane. As the pressure is under 10 MPa, the leakage of the rotor vane accounts for about 50% of the total leakage, but when the pressure is up to 15 MPa, this number comes to 68%.

Author Contributions: Conceptualization, Y.W.; Resources, W.L.; Writing—original draft, Y.W.; Writing—review & editing, Y.W.; Project administration, W.M.; Funding acquisition, J.Z. All authors have read and agreed to the published version of the manuscript.

Funding: This research was funded by Taishan scholars program (Grant No. 202312311) and Shandong Provincial Natural Resources Fund Surface Project (Grant No. ZR202211230116).

Data Availability Statement: The original contributions presented in the study are included in the article, further inquiries can be directed to the corresponding author. All authors have read and agreed to the published version of the manuscript.

Conflicts of Interest: All the authors declare that the research was conducted in the absence of any commercial or financial relationships that could be construed as a potential conflict of interest.

References

1. Nikas, G.K. Eighty years of research on hydraulic reciprocating seals: Review of tribological studies and related topics since the 1930s. *Proc. Inst. Mech. Eng. Part J J. Eng. Tribol.* **2010**, *224*, 1–23. [CrossRef]

2. Dowson, D. Modelling of elastohydrodynamic lubrication of real solids by real lubricants. *Mecc. J. Ital. Assoc. Theor. Appl. Mech.* **1998**, *33*, 47–58.
3. Salant, R.F.; Maser, N.; Yang, B. Numerical Model of a Reciprocating Hydraulic Rod Seal. *J. Tribol.* **2007**, *129*, 91–97. [CrossRef]
4. Xiang, C.; Guo, F.; Liu, X.; Chen, Y.; Jia, X.; Wang, Y. Numerical algorithm for fluid–solid coupling in reciprocating rod seals. *J. Tribol. Int.* **2020**, *143*, 106078. [CrossRef]
5. Yuan, X.; Wang, J.; Lian, Z.; Wang, G. Partial lubrication modeling of reciprocating rod seals based on a developed EHL method. *J. Tribol. Int.* **2021**, *153*, 106585. [CrossRef]
6. Yang, H.-L.; Li, X.; Sun, W.; Deng, F.; Du, J. Mixed EHL numerical analysis and leakage experiment of skeleton reciprocating oil seal. *J. Ind. Lubr. Tribol.* **2021**, *73*, 660–665. [CrossRef]
7. Li, X.L.; Suo, S.F.; Guo, F.; Wu, C.G.; Jia, X.H. A study of reciprocating seals with a new mixed-lubrication model based on inverse lubrication theory. *J. Lubr. Sci.* **2018**, *30*, 126–136. [CrossRef]
8. Cheng, D.; Gu, L.; Sun, Y. Mixed Lubrication Modeling of Multi-Lip Reciprocating Seals Based on Elastohydrodynamic Lubrication Theory. *J. Mach.* **2022**, *10*, 483. [CrossRef]
9. Nikas, G.K.; Sayles, R.S. Study of leakage and friction of flexible seals for steady motion via a numerical approximation method. *J. Tribol. Int.* **2006**, *39*, 921–936. [CrossRef]
10. Qing, H.; Xie, L.X.; Li, L.; Jia, C. Oil film thickness analysis of the sealing surface for hydraulic rotary rectangular vane actuator. *J. Ind. Lubr. Tribol.* **2018**, *70*, 1494–1499. [CrossRef]
11. Nikas, G.K. Performance mapping of rectangular-rounded hydraulic reciprocating seals to minimize leakage, frictional work and abrasive wear with the aid of a duty parameter. *J. Tribol. Int.* **2023**, *179*, 108191. [CrossRef]
12. Nikas, G.K.; Burridge, G.; Sayles, R.S. Modelling and optimization of rotary vane seals. *Proc. Inst. Mech. Engineers. Part J J. Eng. Tribol.* **2007**, *221*, 699–715. [CrossRef]
13. Nikas, G.K.; Sayles, R.S. Modelling and Optimization of Composite Rectangular Reciprocating Seals. *Proc. Inst. Mech. Eng. Part J J. Eng. Tribol.* **2006**, *220*, 395–412. [CrossRef]
14. Ahmed, A.; Masjuki, H.H.; Varman, M.; Kalam, M.A.; Habibullah, M.; Al Mahmud, K.A. An overview of geometrical parameters of surface texturing for piston/cylinder assembly and mechanical seals. *Mecc. J. Ital. Assoc. Theor. Appl. Mech.* **2016**, *51*, 9–23. [CrossRef]
15. Ji, J.; Dong, B.; Fu, H.; Wang, W.; Zhang, Y. Hydrodynamic lubrication of textured infinitely long slider with cross-hatched texture. *J. Mecc.* **2019**, *54*, 2067–2079. [CrossRef]
16. Podgornik, B.; Vilhena, L.M.; Sedlaček, M.; Rek, Z.; Žun, I. Effectiveness and design of surface texturing for different lubrication regimes. *Mecc. J. Ital. Assoc. Theor. Appl. Mech.* **2012**, *47*, 1613–1622. [CrossRef]
17. Shin, J.-H.; Kim, K.-W. Effect of surface non-flatness on the lubrication characteristics in the valve part of a swash-plate type axial piston pump. *Mecc. J. Ital. Assoc. Theor. Appl. Mech.* **2014**, *49*, 1275–1295. [CrossRef]
18. Xiang, C.; Guo, F.; Jia, X.; Wang, Y. Numerical simulation model of reciprocating rod seal systems with axial wear texture on rod surface. *J. Lubr. Sci.* **2023**, *35*, 327–345. [CrossRef]
19. Patir, N.; Cheng, H.S. An Average Flow Model for Determining Effects of Three-Dimensional Roughness on Partial Hydrodynamic Lubrication. *J. Lubr. Technol.* **1978**, *100*, 12–17. [CrossRef]
20. Patir, N.; Cheng, H.S. Application of Average Flow Model to Lubrication Between Rough Sliding Surfaces. *J. Tribol.* **1979**, *101*, 220–229. [CrossRef]
21. Li, L.; Wu, J.B. Deformation and leakage mechanisms at hydraulic clearance fit in deep-sea extreme environment. *J. Phys. Fluids* **2020**, *32*, 1–21. [CrossRef]
22. Suo, H.; Li, G.; Qin, A.; Chen, Z. Simulation analysis of rubber material constitutive model based on Ansys. In Proceedings of the 2023 3rd International Conference on Industrial Manufacturing and Structural Materials (IMSM 2023), Guangzhou, China, 17–19 February 2023; Volume 2541, p. 012007.